Notes

Using Thermal Infrared Cameras to Detect Avian Chicks at Various Distances and Vegetative Coverages

Diann J. Prosser,* Tom Collier, Jeffery D. Sullivan, Katherine E. Dale, Carl R. Callahan, Peter C. McGowan, Edwin J. Gaylord, Julia M. Geschke, Lucas Howell, Paul R. Marban, Saba Raman

D.J. Prosser
U.S. Geological Survey, Patuxent Wildlife Research Center, 12100 Beech Forest Road, Laurel, Maryland 20708

T. Collier
UASBio,llc, 12139 Patapsco Ridge Road, Marriottsville, Maryland 21104

J.D. Sullivan
Natural Systems Analysts, 1598 Winter Park, Florida 32789

K. Dale
UC Santa Cruz, 130 McAllister Way, Santa Cruz, California 95060

C.R. Callahan, P.C. McGowan
U.S. Fish and Wildlife Service, Chesapeake Bay Field Office, 177 Admiral Cochrane Drive, Annapolis, Maryland 21401

E.J. Gaylord, J.M. Geschke, L. Howell, P.R. Marban, S. Raman
University of Maryland, 72940 Baltimore Avenue, College Park, Maryland 20740

Abstract

Population monitoring of nesting waterbirds often involves frequent entries into the colony, but alternative methods such as local remotely sensed thermal imaging may help reduce disturbance while providing a cost-effective way to survey breeding populations. Such an approach can have high initial costs, however, which may have reduced the number of studies investigating functionality of paired thermal infrared camera and small unmanned aerial systems. Here, we take the first step of exploring the ability of two thermal infrared cameras to detect an avian chick under varying vegetative cover and distances, preceding field-mounting applications on a small unmanned aerial system. We created seven ''bioboxes'' to simulate a range of natural vegetation types and densities for a globally important colonial ground-nesting waterbird species, the common tern *Sterna hirundo*. We placed a juvenile chicken *Gallus gallus* (surrogate for the locally endangered common tern) in each box, and we tested two market-accessible infrared cameras (produced by FLIR Systems and Infrared Cameras, Inc.) at five elevations using a stationary boom (maximum height = 12 m). We applied computer-based digital thresholding to collected images, identifying pixels meeting one of seven threshold values. The chick was visible from at least one threshold value in 19 and 31 of 35 processed by the FLIR Systems and Infrared Cameras, respectively. Percentage of the chick identified across thresholds was generally highest at lower threshold values and elevations and decreased as elevation and threshold increased; however, the relative importance of each variable changed dramatically across bioboxes and camera types. Ability to detect a chick from processed images generally decreased with increasing elevation, and although we made no quantitative comparisons among boxes, detectability appeared greatest in images from both cameras when little or no vegetation was present. Interestingly, no single threshold value was best for all bioboxes. We observed notable differences between cameras including visual resolution of detected temperature differentials and image processing speed. Results of this controlled study show promise for the use of thermal infrared systems for detecting cryptic species in vegetation. Future research should work to combine thermal infrared and visual sensors with small unmanned aerial systems to test applicability in a mobile field application.

Keywords: chick; common tern; drone; population monitoring; thermal infrared; UAS; *Sterna hirundo*

Received: August 1, 2019; Accepted: January 2, 2020; Published Online Early: January 2020; Published: June 2020

Citation: Prosser DJ, Collier T, Sullivan JD, Dale KE, Callahan CR, McGowan PC, Gaylord EJ, Geschke JM, Howell L, Marban PR, Raman S. 2020. Using thermal infrared cameras to detect avian chicks at various distances and vegetative

coverages. *Journal of Fish and Wildlife Management* 11(1):245–257; e1944-687X. https://doi.org/10.3996/072019-JFWM-062

* Corresponding author: dprosser@usgs.gov

Introduction

Researchers' efforts to obtain data regarding adult and chick abundance, nest counts, or hatching and fledging success using conventional methods can be difficult, time consuming, and potentially disruptive for wild birds (Carney and Sydeman 1999). For example, cryptic coloration and behavior of many juvenile waterbirds make detection challenging and may lead to underestimation (Steinkamp et al. 2003). Visual surveys or resighting events using spotting scopes are known to have an inherent bias as vegetation grows across a season, making birds more difficult to see, which can alter results across sites or season (Bibby and Buckland 1987). Similarly, chick or nest searching may be time intensive, yet prolonged human presence in a colony of nesting waterbirds is to be avoided given the potential for disturbance such as adult flush (temporary colony evacuation leaving eggs or chicks exposed), altering of foraging behavior, triggering of juveniles to evacuate the nest, or nest abandonment (Palmer 1941; Erwin 1989; Rodgers and Smith 1995). Data obtained from reproductive surveys are necessary for population assessment and development of management plans for declining species such as the common tern *Sterna hirundo*, which is listed as endangered within the state of Maryland (Maryland Natural Heritage Program 2016). To help balance the need for data and potential disturbance caused by acquiring such data, researchers are continually searching for population survey techniques that are both less invasive and less costly.

Thermal infrared imaging (TIR) is one method that has received significant attention in recent years as an option for surveying wildlife while reducing disturbance relative to traditional methods. As explained in a review by McCafferty (2013), TIR has been examined as a means by which researchers can study cryptic avian species (Locke et al. 2006; Mills et al. 2011; Andes et al. 2012), nesting locations and densities (Boonstra et al. 1995; Benshemesh and Emison 1996; Galligan et al. 2003; Kinzel et al. 2006), migration ecology (Betke et al. 2008; Mirzaei et al. 2012), and thermoregulatory behaviors (McCafferty et al. 1998). However, the majority of studies involving TIR have used handheld devices during ground surveys, which does not reduce entry into the colony (McCafferty 2013). One potential approach to minimize disturbance is to affix a TIR camera onto a small unmanned aircraft system (sUAS) and capture imagery semiremotely. Because sUAS units weigh less than 25 kg (rule 14 CFR part 107), they are optimal for transport and deployment by a single operator. Recent studies by Chabot and Bird (2012), Chabot et al. (2015), Hodgson et al. (2016), and Reintsma et al. (2018) successfully used a sUAS to survey Canada geese *Branta canadensis* and common terns with minimal disturbance. Although these studies used a visual survey system other than TIR and concentrated on surveying adults, they demonstrate the potential for this approach. Additionally, pairing sUAS and TIR presents the opportunity to survey for individuals that are difficult to detect. For instance, older tern chicks that have left the nest pose a significantly greater detection challenge than adults when using traditional approaches because they are small and often cryptically colored, well insulated, and may hide under vegetation to obtain shade and avoid predation (Jenks-Jay 1982).

To our knowledge, the only works that have combined TIR and sUAS to examine wild birds were for surveying mid-size or large species in open habitat (Hutt 2011; Owen 2011; Hanson et al. 2014). The paucity of research on the practicality of this approach for smaller species is likely driven by the high initial costs. TIR units tested in this study cost between US $10,000 and $12,000, and the sUAS (with peripheral equipment) required to carry them had a similar price tag. Additionally, the use and exportation of TIR sensors may be subject to more stringent governmental regulations because of their use in civil and military applications (Linchant et al. 2015).

Because of the lack of experimentation, there is justifiable skepticism in the literature as to the effectiveness of TIR for use in dense vegetation, for surveying birds in warm climates, for detecting well-insulated species, and for use during daytime (Boonstra et al. 1995; Butler et al. 2006; Steen et al. 2012). Thus, research aimed at verifying the ability of TIR systems to detect avian chicks in a variety of vegetative conditions was needed to serve as a proof of concept and stimulate additional research into pairing TIR and sUAS. The objectives of this study were to 1) determine the extent to which two available TIR sensors were able to detect a juvenile domestic chicken, *Gallus gallus* (used as a surrogate for a tern chick) in various vegetation types and from multiple elevations above the subject during diurnal hours; 2) examine if computer-based digital thresholding could allow users to successfully detect

Table 1. Vegetative makeup of bioboxes used to simulate realistic common tern *Sterna hirundo* nesting habitats. We then placed a domestic chicken chick *Gallus gallus* in each box and photographed them with two different thermal cameras to examine detectability across a range of elevations, vegetative coverages, and image processing thresholds. Whereas we conducted work in Millersville, Maryland on 9 June 2015, we obtained plants and sand from Poplar Island, a dredge material restoration site in the Chesapeake Bay.

Biobox	Vegetation temperature (difference from ambient, °C)	Vegetation density[a]	Species
A	—	—	No cover
B	−2.5	Sparse	Saltmeadow cordgrass (*Spartina patens)*
C	−2.17	Medium	Saltmeadow cordgrass (*Spartina patens)*
D	−2.36	Dense	Saltmeadow cordgrass (*Spartina patens)*
E	−1.74	Dense	Sea rocket (*Cakile edentula*)
F	−2.28	Medium	Mixed saltmeadow cordgrass (*Spartina patens*) and smooth cordgrass (*Spartina alterniflora*), sea rocket (*Cakile edentula*), and ragweed (*Ambrosia* spp.)
G	−2.74	Sparse	Milkweed (*Asclepsias* spp.)

[a] Volume densities are as follows: sparse = 30% aerial cover, medium = 60% aerial cover, dense = 90% aerial cover.

the thermal signature of the chick; 3) compare and contrast the capabilities and efficacy of the two TIR systems to determine potential for use in detecting tern chicks in the field; and 4) examine the implications of our results on the potential for future use of TIR cameras with sUAS systems. It is our hope that this study can lay the groundwork for further research into the paired use of sUAS and TIR systems.

Methods

Sensor information

We compared two TIR cameras during this study, both of which operate in the 8- to 15-μm long-wave IR wavelength range. The first, a forward-looking IR (FLIR) camera, was a FLIR Tau-1 (FLIR Systems, Wilsonville, OR); it had an f-1.2 fixed focal-point lens with 13-mm zoom and a 17-μm-pixel pitch, combined with a 640 × 512 pixel microbolometer detector array, a Tau virtual private cloud module with universal serial bus and video cables, and FLIR camera controller geographical user interface software version 1.0.0.114. The FLIR Tau-1 was approximately 44.5 × 44.5 × 44.5 mm and weighed 72 g with the lens attached.

The second camera was an Infrared Cameras, Inc. (ICI) 9640 (Beaumont, TX); it had an f-1.0 lens with 12.5-mm zoom and a 17-μm-pixel pitch, a 640 × 480 pixel microbolometer detector array, a universal serial bus interface module, and ICI IRFlash software version 2.15.5.18. The ICI 9640 measured approximately 34 × 30 × 34 mm and weighed 110 g with the lens attached. Both lenses had fixed f-stops and shutter speeds and were factory calibrated for their respective cameras. For both cameras, we completed all adjustments to noise, contrast, color palettes, and other parameters postcapture.

We used a GoPro Hero 3+ camera (GoPro, Inc., San Mateo, CA) with a Peau Productions 8-mm lens (Peau Productions, San Diego, California) alongside the TIR cameras to capture visual images of the study. We used laptops and an iPad (Apple, Inc., Cupertino, CA) to run the camera software and to view images in real time. All cameras and associated technologies and services were provided by UASBio, llc (Marriottsville, MD), and are practical for use with sUAS systems as described.

Trials

We conducted trials outdoors in Marriottsville, Maryland on 9 June 2015 from 1400 to 1700 hours Eastern Standard Time. We used a 12.8-m boom lift to raise the camera systems to 3, 6, 9, 10.5, and 12 m above the subject matter. Attached to the lift box was a wooden platform carrying the two TIR cameras, a high-definition visual camera, laptops for dynamically processing the TIR images using software provided by the respective camera manufacturers, and viewing monitors. Although we recognize that drones may need to fly at higher elevations than those tested in this study, we were limited by the abilities of our boom lift and felt that the elevations selected would provide the best examination of the potential of this pairing for success.

We constructed seven bioboxes using rectangular plastic buckets measuring 0.4 × 0.5 × 0.4 m, and filled each with sand and vegetation collected from the Paul S. Sarbanes Ecosystem Restoration Project at Poplar Island, an important nesting site for common terns in the Chesapeake Bay where the results of this experiment may be applied. The seven bioboxes had vegetation coverages ranging from no vegetation to > 90% cover (Table 1, Figure 1). Vegetation types included saltmeadow cordgrass *Spartina patens*, smooth cordgrass *Spartina alterniflora*, sea rocket *Cakile ednunata*, ragweed *Ambrosia* sp., and milkweed *Asclepsias* sp., all of which are commonly found within or near the common tern colony on Poplar Island. The combination of vegetation types and densities was meant to best replicate realistic field conditions. We placed a 7-d-old domestic chicken (hereafter, chick) weighing 68.0 g and measuring ~50 mm × 75 mm inside an IR-neutral plastic cup to keep it stationary within each biobox. We used the same chick throughout the experiment. Domestic chicken chicks are ideal surrogates for terns, as they are easily obtainable and are roughly the same size as a juvenile common tern. Additionally, both chicken and common tern chicks

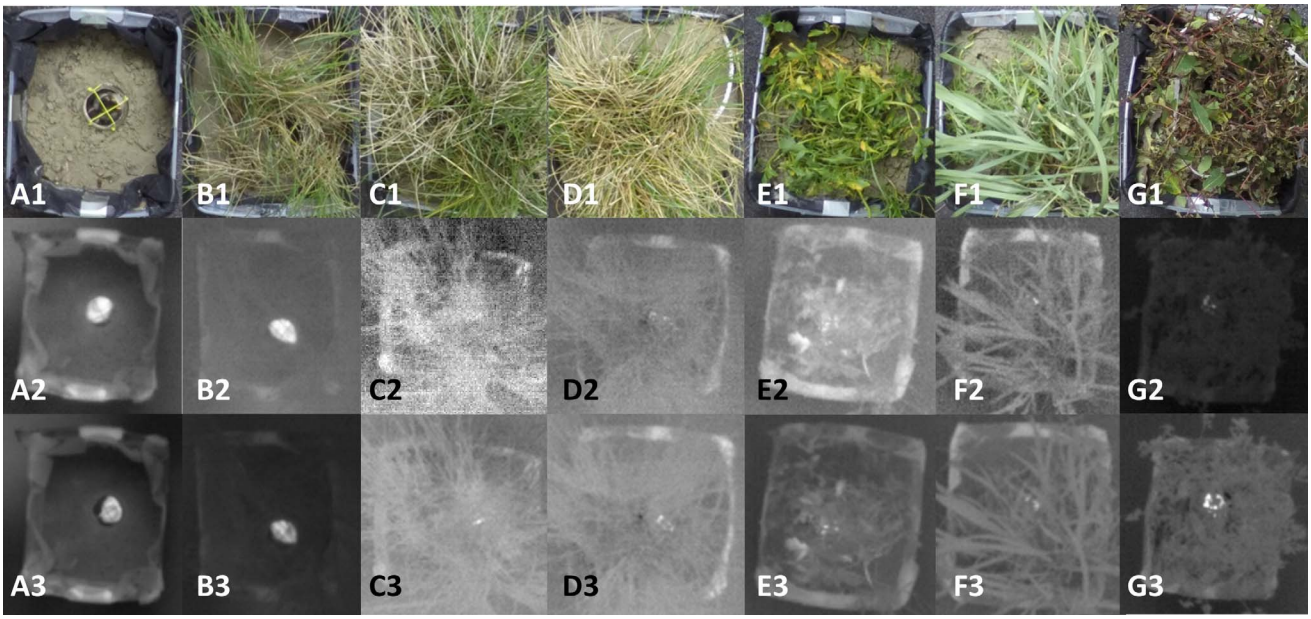

Figure 1. Representative images of seven bioboxes with chicken chick *Gallus gallus* from 3 m above the substrate of the box. Vegetation types are as follows: (**A**) no cover; (**B**) sparse saltmeadow cordgrass *Spartina patens*; (**C**) medium saltmeadow cordgrass; (**D**) dense saltmeadow cordgrass; (**E**) dense sea rocket *Cakile edentula*; (**F**) medium mixed grasses and forbs, including saltmeadow cordgrass and smooth cordgrass *Spartina alterniflora*, sea rocket, and ragweed *Ambrosia* sp.; (**G**) sparse milkweed *Asclepsias* sp. Sparse = 30% cover, medium = 60% cover, and dense = 90% cover. Images A2–G2 are from the FLIR Systems Tau-1 camera; A3–G3 are from the Infrared Cameras, Inc. 9640. We collected images in Millersville, Maryland on 9 June 2015 to examine detectability across a range of elevations, vegetative coverages, and image processing thresholds.

are semiprecocial and covered in down at hatching (Nisbet et al. 2017; Chen et al. 2019), with the integuments of common tern chicks and other gallinaceous chicks composed of comparable amounts of water and equaling comparable proportions of the chicks' overall body (Ricklefs 1979). Thus, we believe there should be limited differences in the detectability of the two species via a TIR camera.

We positioned each biobox directly underneath the camera array and raised the lift to the prescribed heights. We obtained photos of the bioboxes from each of the cameras at every elevation (3, 6, 9, 10.5, and 12 m). Because of differences in processing speed, we took three consecutive replicate photos using the ICI camera and only one using the FLIR camera. We recorded the ambient temperature and general weather conditions (sunny or otherwise) and used a handheld FLIR-TG165 imaging IR thermometer to measure the surface temperature of the vegetation, sand, and chick.

Digital thresholding

We used digital thresholding to quantify the thermal signature of the chick across bioboxes and elevations. Pixel brightness is denoted by a value from 0 to 255, where zero is absolute black and 255 is white. In digital thresholding, all pixels with values above or below a specific threshold are selected, with values not meeting the selection criteria ignored. Here, we wrote a simple Python script (Python Software Foundation, Wilmington, DE) to repeatedly query each photo to select pixels with values greater than or equal to thresholds 115, 130, 145, 160, 175, 190, and 205. Each query produced a new raster file that could then be overlaid on the original photo in ArcMap 10.6 (ESRI, Inc., Redlands, CA).

Image analysis

ICI image comparison. We selected 14 sets of the replicate ICI images and clipped each image down to just the inside of the biobox so that we removed all uncontrolled environmental factors. We then compared each of the three clipped images within each image set by calculating the root mean-square error of the pixel values. We selected this approach as it would allow for direct comparison of values and not just identification of correlation (i.e., are warmer areas the same between pictures even if actual pixel values are different). We conducted this exercise to determine if a single ICI image from each biobox/elevation/threshold combination was representative of the three taken at that combination, or if individual examination was warranted. Once we confirmed that ICI replicates were comparable (see Results), we used only the first image of each ICI image set for subsequent analyses.

Percentage of chick selected. After ICI image comparison we examined the number of pixels in each processed image selected within the chick's thermal signature using the Image Analysis tool in ArcMap. In the majority of photos, the thermal signature of the chick

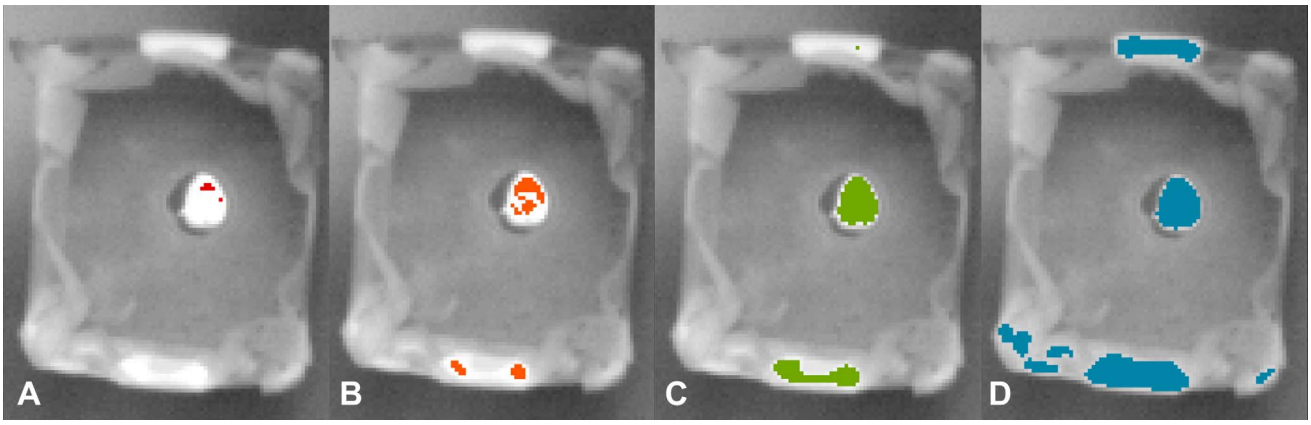

Figure 2. Digital processing results for a chicken chick *Gallus gallus* in biobox A (no vegetative cover) across thresholds (**A**) 205, (**B**) 175, (**C**) 145, and (**D**) 115. We took the photo at 3-m elevation using the Infrared Cameras, Inc. 9640. Note that although thresholds 145 and 115 produced the most complete representation of the chick's thermal signature, we also selected nonchick pixels within the biobox using these threshold values. We collected images in Millersville, Maryland on 9 June 2015 to examine detectability across a range of elevations, vegetative coverages, and image processing thresholds.

was distinct from surrounding pixels, and this could be completed visually (Figure 2). For cases in which too many pixels were selected within the biobox to discern which pixels formed the chick (Figure 3), we recorded the selected chick area as equal to the maximum chick area. We calculated maximum chick area based on the number of pixels required to display the chick fully at a given elevation per camera, and determined it via the following formula where all inputs are in millimeters and all outputs in pixels:

$$\text{Length}^i = \frac{\left(\frac{\text{length of subject}}{\text{distance from subject}}\right) \times \text{zoom}}{\text{pixel pitch}};$$

$$\text{Width}^i = \frac{\left(\frac{\text{width of subject}}{\text{distance from subject}}\right) \times \text{zoom}}{\text{pixel pitch}};$$

$$\text{Maximum chick area} = \text{length}^i \times \text{width}^i.$$

Once we determined the number of chick pixels selected at a given threshold, we calculated the percentage of the chick selected via thresholding as

$$\text{Percentage of chicks selected} = \frac{\text{pixels selected(within chick's thermal signature)}}{\text{maximum chick area}}.$$

We felt that it was necessary to always calculate percentage selected as a function of the maximum number of pixels the chick could excite because there was no way to tell if the chick's thermal signature in each image truly represented the whole animal. This approach allowed our calculations to be standardized across images, even when the chick was covered by vegetation and not visible within the paired GoPro image.

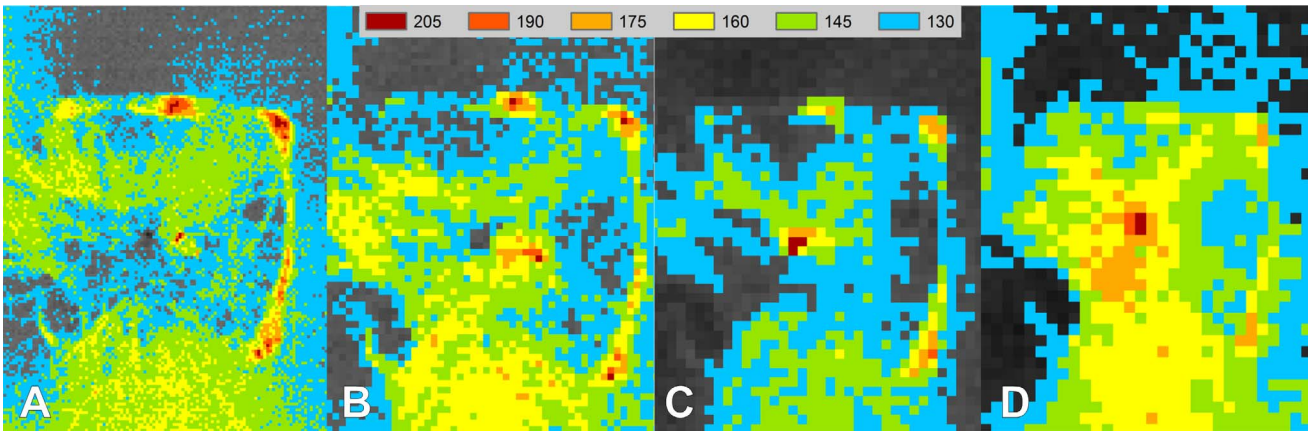

Figure 3. Digital processing results for Infrared Cameras, Inc. 9640 camera images of biobox D (dense saltmarsh cordgrass *Spartina patens*) across elevations (**A**) 3 m, (**B**) 6 m, (**C**) 9 m, and (**D**) 12 m. Threshold is represented by color, with the highest threshold values represented by the warmest parts of the image. The chicken chick *Gallus gallus* is visible in the middle of the photo as the "hottest" spot. We collected images in Millersville, Maryland on 9 June 2015 to examine detectability across a range of elevations, vegetative coverages, and image processing thresholds.

Chick detection. For every processed image we recorded whether the chick could be manually detected by a human observer before digital thresholding. We then repeated this at every threshold value, recording if the chick was visible (i.e., a human observer could identify the selected pixels as the chick), not selected at all, or if too many pixels were selected to identify the chick. Although examining the percentage of chick selected via thresholding provides information regarding whether the camera was able to indicate the presence of the chick at all, this additional approach examines if the depiction of the chick created via thresholding is sufficient for an observer to actually identify the chick in the processed image.

Statistical analysis. To examine the differences in the percentage of the chick selected and ability to detect a chick postprocessing across our array of images we constructed a suite of 65 beta regression (using logit link function) and binomial regression models, respectively. Because beta regression (Cribari-Neto and Zeileis 2010) requires data bound between 0 and 1, instances where 0% or 100% of a chick's maximum area was detected were mutated via the formula $x' = (x(N - 1) + s)/N$ (Smithson and Verkuilen 2006), where N is sample size and s is a numerical constant set to 0.5. All models consisted of fixed effects for camera type, elevation, biobox, and threshold, with all possible combinations of one-way interactions between these fixed effects included in the model suite. Although threshold appears to be a continuous variable it is treated categorically because of the range of values used in making a non-linear relationship between detection and threshold likely. We used the Akaike information criterion selected for small sample size to select the best-fit model for percentage of chick selected and chick detection independent of each other. We performed all analyses in R 3.4.2. Complete raw data are available in Data A1 (*Archived Material*).

Results

On the day we conducted the trials, it was cloudy and the ambient temperature was 19.1–20.0°C. The average vegetation temperature was 17.0°C and average sand temperature was 17.2°C. On average, box E (dense sea rocket) had the warmest vegetation, at only 1.7°C cooler than the ambient temperature (Table 1). Box G (sparse milkweed) had the coolest vegetation, at 2.7°C cooler than ambient. Seven bioboxes and five elevations led to 35 different possible combinations per camera and 140 total TIR images (three photos from the ICI camera and one photo from the FLIR camera per combination).

ICI image comparison

We compared the pixels selected in 14 of the total 35 ICI image sets (the series of three images collected at every elevation/biobox combination) at all threshold levels. We selected replicates from biobox C (3, 6, 9, 10.5, and 12 m), biobox E (6 and 9 m), biobox F (3, 6, and 9 m), and biobox G (3, 6, 9, and 10.5 m). The mean value of the root mean-square error for all comparisons was 5.10 and ranged from 2.02 to 24.45 (Table S1, *Supplemental Material*). As the highest root mean-square error was 9.69% and the mean was 2% of the possible range of pixel values (0–255), we considered images within an ICI image set to be comparable.

Percentage of chick selected via thresholding

We compared a suite of 65 candidate models to explain trends in the percentage of a chick's area selected in each image using fixed effects for camera type, threshold, elevation, and biobox along with every possible combination of one-way interactions between these variables. After model comparison we found that the best-fit model was the following: percentage detected $\sim$ camera + elevation + threshold + box.letter + camera:elevation + camera:threshold + camera:box.letter + elevation:box.letter (Table S2, *Supplemental Material*). For both the ICI and FLIR cameras, the percentage of the chick selected via thresholding was generally highest at lower threshold values and elevations (Figure 4; Figure S1, *Supplemental Material*; Table S3, *Supplemental Material*) and decreased as elevation and threshold increased. However, the relative importance of each variable changed dramatically across bioboxes and camera types. For instance, elevation affected selection percentage significantly more for the FLIR camera than for the ICI cameras ($P < 0.05$).

Chick detection from processed images

Unfortunately, although a high percentage of a chick may have been selected in a given image, that did not mean that the chick could actually be identified from the processed images. It was common for too many pixels to be selected at lower thresholds, causing the image to appear "washed out" so the chick could not be differentiated from other selected pixels. The chick was visible from at least one threshold value of 19 FLIR and 31 ICI images of a possible 35 (Figure 5). Comparatively, the chick was visible in 29 FLIR and 32 ICI images of the 35 raw images.

We compared a suite of 65 candidate models to explain trends in whether a chick could be detected after processing each image using fixed effects for threshold, elevation, and biobox along with every possible combination of one-way interactions between these variables. After model comparison we found that the best-fit model was the following: visible $\sim$ camera + elevation + threshold + box.letter + camera:elevation + camera:box.letter + elevation:box.letter + threshold:box.letter (Table S4, *Supplemental Material*). Detectability generally decreased with increasing elevation, and although we made no qualitative comparisons among boxes, detectability appeared greatest for both ICI and FLIR when little or no vegetation is present (Figure 6; Table S5, *Supplemental Material*). Of interest, no single threshold value was best for all bioboxes.

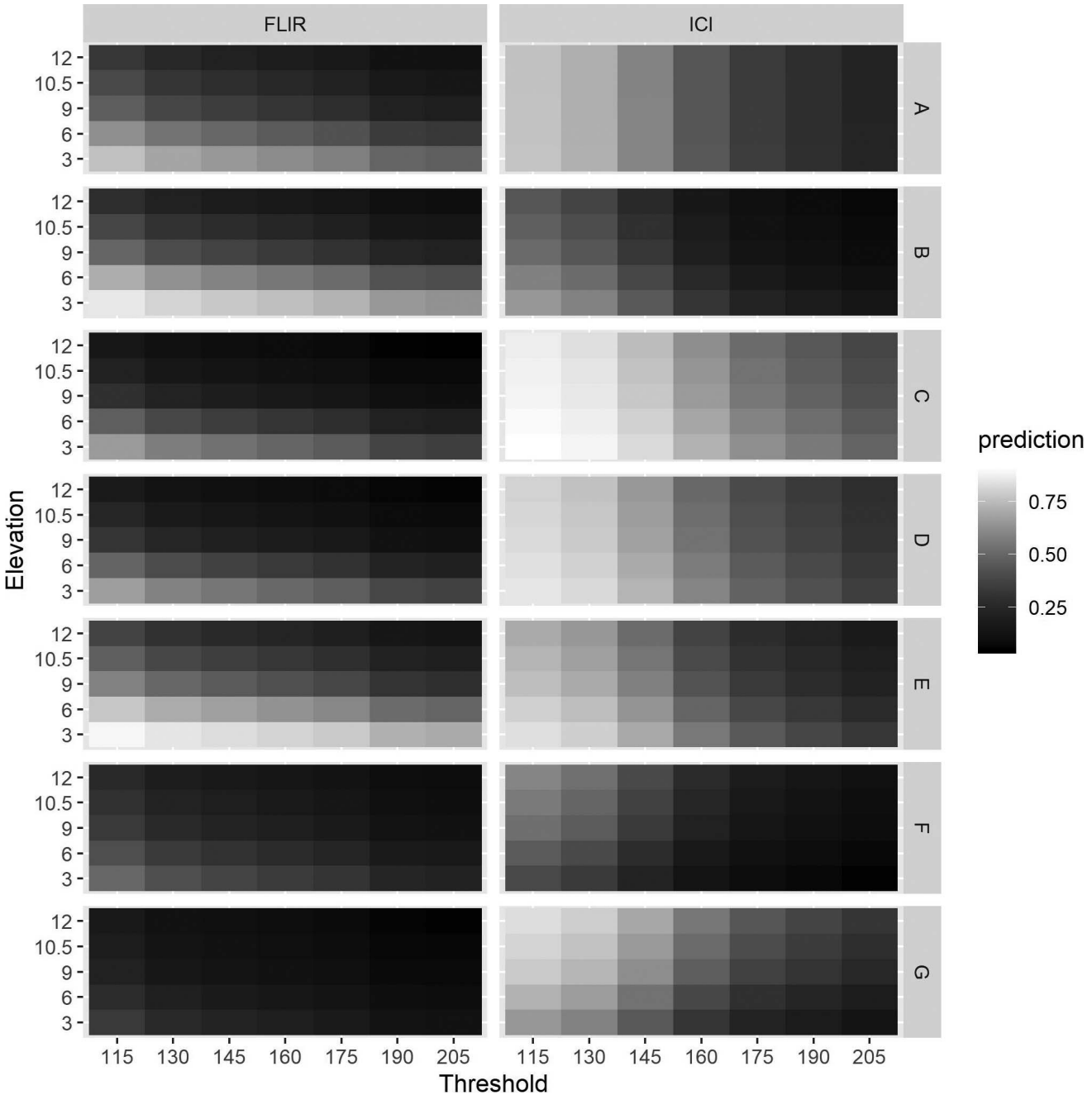

Figure 4. The model-fitted values of the percentage of a domestic chicken chick *Gallus gallus* selected by FLIR Systems Tau-1 and Infrared Cameras, Inc. 9640 cameras as explained by varying elevation (in meters), threshold, and vegetation levels. The vegetation types are as follows: (**A**) no cover; (**B**) sparse saltmeadow cordgrass *Spartina patens*; (**C**) medium saltmeadow cordgrass; (**D**) dense saltmeadow cordgrass; (**E**) dense sea rocket *Cakile edentula*; (**F**) medium mixed grasses and forbs, including saltmeadow cordgrass and smooth cordgrass *Spartina alterniflora*, sea rocket, and ragweed *Ambrosia* sp.; (**G**) sparse milkweed *Asclepsias* sp. Sparse = 30% cover, medium = 60% cover, and dense = 90% cover. We collected images in Millersville, Maryland on 9 June 2015.

Discussion

The results we report in this study have positive implications for the use of TIR + sUAS systems for avian surveys. Perhaps the most promising result was the ability to detect the chick both before and after digital processing in the majority of photos despite the fact that testing occurred during fairly warm diurnal hours and with a small target individual. Although the percentage of chick selected decreased with the addition of dense vegetation, the ability to detect the chick from at least one threshold value at most biobox and elevation combinations suggests that this approach could be used across a variety of habitats. It would be especially well suited for species such as common terns that are often found in limited vegetation. Although the trends we

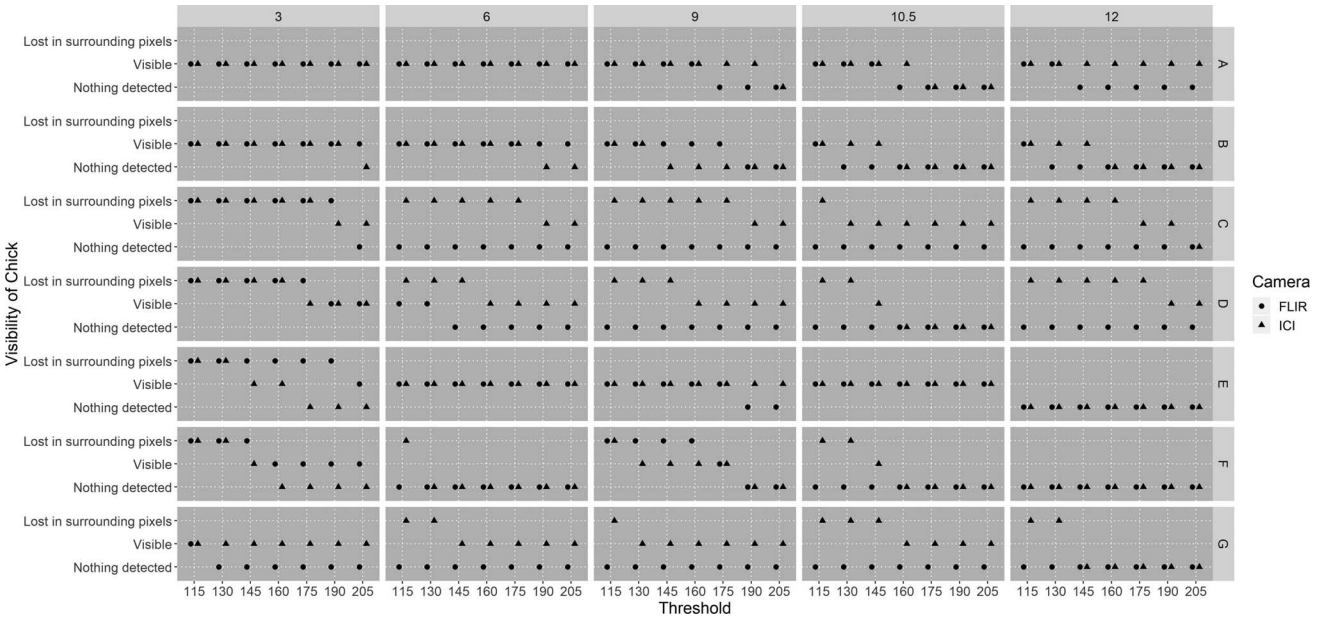

Figure 5. Visibility, to a human observer, of a domestic chicken chick *Gallus gallus* in digitally processed images captured by FLIR Systems Tau-1 and Infrared Cameras, Inc. 9640 cameras as explained by varying elevation (in meters), threshold, and vegetation levels. The vegetation types are as follows: (**A**) no cover; (**B**) sparse saltmeadow cordgrass *Spartina patens*; (**C**) medium saltmeadow cordgrass; (**D**) dense saltmeadow cordgrass; (**E**) dense sea rocket *Cakile edentula*; (**F**) medium mixed grasses and forbs, including saltmeadow cordgrass and smooth cordgrass *Spartina alterniflora*, sea rocket, and ragweed *Ambrosia* sp.; (**G**) sparse milkweed *Asclepsias* sp. Sparse = 30% cover, medium = 60% cover, and dense = 90% cover. We collected images in Millersville, Maryland on 9 June 2015.

observed in this study are promising, we did identify several factors that warrant careful consideration when designing future studies that utilize a combined TIR + sUAS approach.

One of the first elements that must be considered when designing a TIR + sUAS approach is the type of TIR system that will be used. Although detector specifications are identical in the two TIR systems tested, at the time of our study the lens system, camera processor, interface, and software of the ICI system combined to produce clearer and more consistent results than the FLIR camera. In our study, the FLIR camera produced darker photos of lower contrast, which subsequently led to a dimmer chick signature and subsequent reduced functionality, especially at 10 and 12.2 m. Our results indicated that the ICI camera generally detected a greater proportion of the chick's thermal signature across bioboxes and elevations than the FLIR camera, though this also made it more prone to selecting too many pixels, preventing chick identification postprocessing. Still, the ICI camera allowed the greatest detection of chicks across threshold, vegetation types, and elevations. Additionally, the ICI camera system processed images more quickly than the FLIR system, at a ratio of about 3 to 1, increasing the likelihood of detecting a moving bird. It is encouraging that ICI replicate photos were comparable, as variation would undermine the robustness of using TIR to obtain consistent results. In this competitive field, innovation and technical changes occur frequently. In selecting a TIR system, the user may be well served to carefully compare detectors, lenses, sUAS compatibility, power requirements, image transmission, and camera controls of multiple TIR models available at the time of purchase.

Another important factor to consider before utilizing a TIR + sUAS approach is the habitat of the area to be surveyed. Although we did not directly examine the role of vegetation density or morphology, a qualitative review of our findings indicates that the plant physiology/growth pattern may be just as important to detectability as sheer vegetation volume. Certain varieties of plants have physiological characteristics shown to inhibit thermal transmittance, either through a high rate of reflectance or absorbance. For instance, sea rocket has thick, waxy leaves, morphological characteristics that have been shown to increase the absorption of IR radiation (Gates et al. 1965; Mulroy 1979). Unsurprisingly, we found sea rocket to have the highest temperature of any vegetation used in this study. Other plant characteristics such as thick stems may also act as a barrier to IR. For instance, although we classified the total cover of milkweed in biobox G as sparse, we could not discern the thermal signature of the chick at high elevations for either camera type. However, it does not appear as though vegetation density and morphology influence chick detectability uniformly across camera types. We suggest that dense vegetation is less of a limitation for the ICI camera because of the generally higher "brightness" of images from this source, potentially affording this camera type better detectability as the growing season progresses.

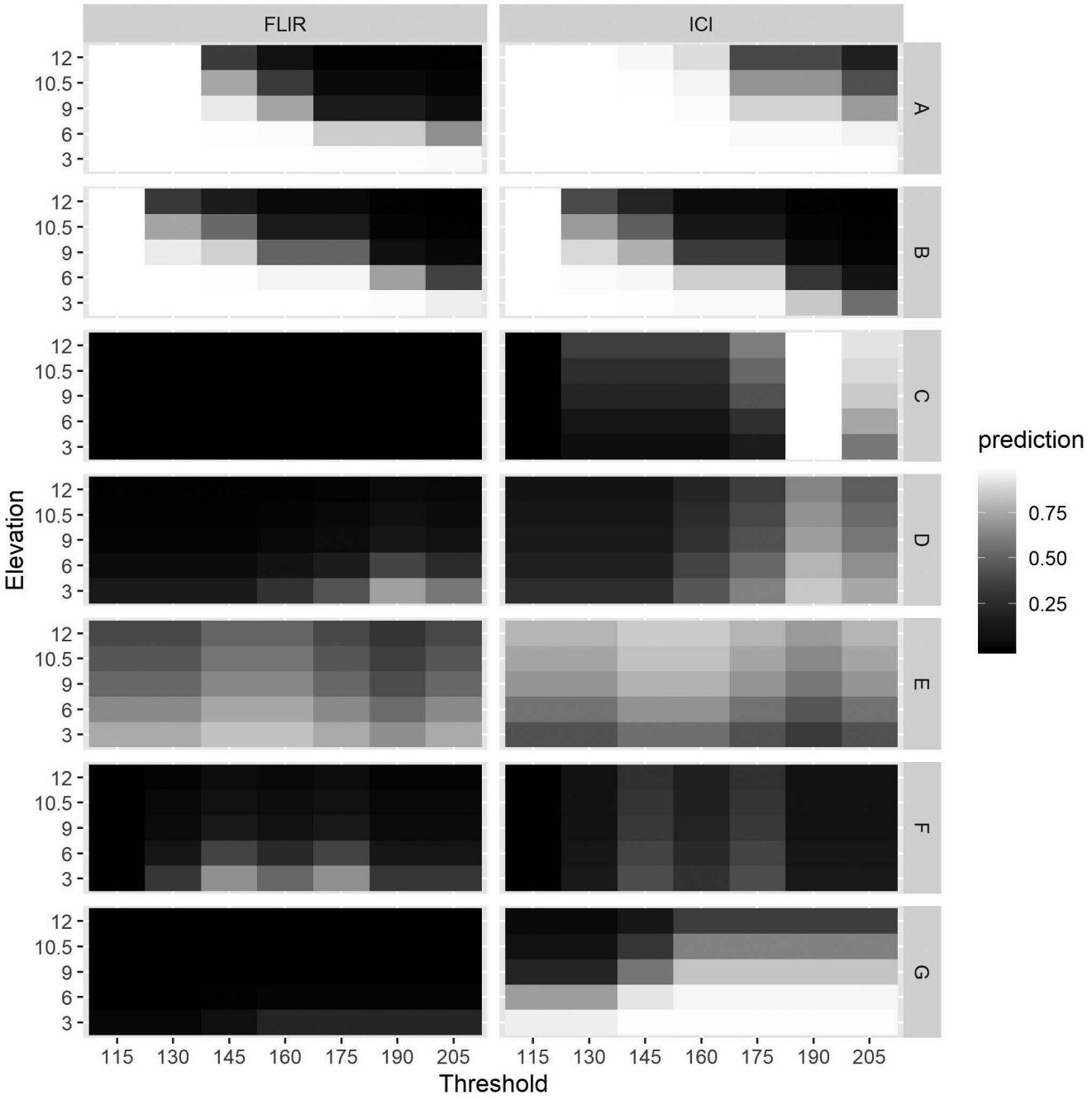

Figure 6. Model-fitted values of the visibility, to a human observer, of a domestic chicken chick *Gallus gallus* in digitally processed images captured by FLIR Systems Tau-1 and Infrared Cameras, Inc. 9640 cameras as explained by varying elevation (in meters), threshold, and vegetation levels. Vegetation types are as follows: (A) no cover; (B) sparse saltmeadow cordgrass *Spartina patens*; (C) medium saltmeadow cordgrass; (D) dense saltmeadow cordgrass; (E) dense sea rocket *Cakile edentula*; (F) medium mixed grasses and forbs, including saltmeadow cordgrass and smooth cordgrass *Spartina alterniflora*, sea rocket, and ragweed *Ambrosia* sp.; (G) sparse milkweed *Asclepsias* sp. Sparse = 30% cover, medium = 60% cover, and dense = 90% cover. We collected images in Millersville, Maryland on 9 June 2015.

Although the physical systems and their applicability to a given study area must be considered before data collection, the selection of a threshold level for digital thresholding can be performed in the laboratory. We determined no single threshold value to be quantitatively "best" for analyzing the photos, although thresholding results using values 130 through 190 typically handled the trade-off between sensitivity and accuracy best. The ideal result of thresholding is for all detected pixels to fall within the chick's thermal signal. In reality, using simple thresholding to distinguish a defined, complete image of the chick while simultaneously detecting no other pixels in the image is difficult. This is especially true for field-based images, where objects

such as trees, rocks, and roads have strong heat signatures of their own. In this small-scale experiment, it was easy to visually identify the chick and differentiate its thermal signature from surrounding pixels, even at the higher elevations and with a variety of vegetation types. Identification was also easier because of our knowledge of the chick's general location and the absence of objects within the biobox that were emitting IR radiation to the same degree as the chick. In future studies, examination of a researcher's field site may help inform the choice of threshold, though the best approach may be to process colonies in segments, applying different threshold values as needed. Additionally, because chicks were visible from raw images more frequently than from thresholding, it may appear logical to count chicks only from raw TIR images; however, users must remember that we conducted this study on a very small area. In practical scenarios manual counting could be very time intensive and subjective; however, approach should not be completely discounted if feasible as it at least warrants thorough consideration.

Unfortunately, when TIR images are captured in the field, researchers will not have the benefit of prior knowledge to aid in the differentiation between target species and false positives. A simple approach to increase certainty in identification is to conduct surveys at an elevation that minimizes disturbance while allowing for necessary image detail. If surveys must be conducted at higher elevations because of disturbance concerns, detection can be improved by using a longer lens—focal lengths are available up to 60 mm; however, as size increases, the field of view constricts, requiring more flight time to completely survey a given area. Additionally, researchers can apply image-editing and pattern-recognition algorithms to remove extraneous background signatures and isolate thermal signatures of any birds present. Such approaches have proven useful for detecting bats (Betke et al. 2007; Hristov et al. 2008) and distinguishing them from birds (Mirzaei et al. 2012, 2014), as well as for identifying birds in drone-mounted camera footage (Abd-Elrahman 2005). Precapture image filtering, which forces thermal signatures to stand out amid background noise, has also proven to be a viable method for reducing false positives (Steen et al. 2012).

In addition to false positives, other potential factors to consider when pairing TIR and sUAS equipment in a true field setting include thermal loading, motion and vibration, wind, and the dynamics of field operations. The effects of these variables are not exclusively beneficial or harmful—for example, wind could move vegetation, revealing a hidden chick, or it could hinder an observer's ability to pinpoint the thermal signature of a chick beneath a moving plant. However, thermal loading will likely be the most significant problem to cope with and could require that sUAS/TIR surveys be conducted early in the day (Butler et al. 2006). Still, sensitive detectors and computer algorithms should be able to distinguish among endothermic organisms, plants, and inorganic materials based on emissivity differences, even if objects are precisely the same temperature. Furthermore, additional research into the use of paired sUAS and TIR technology for breeding colony surveys is needed to understand the ability of this approach to determine brood size. Although we examined the ability to detect a single chick, we did not try to determine if brood size could be accurately calculated using this approach.

Detecting terns, especially elusive chicks that have left the nest, is a challenging endeavor. We conclude that the use of TIR paired with sUAS has potential to improve detection and decrease human disturbance to a colony of nesting waterbirds. The myriad of potential modifications involved makes the system functional across many applications. This study suggests that for successful use in the field, more complex pre- and postprocessing will be required. Further studies will need to examine the accuracy of this technique for detecting nests, eggs, and adults in the field.

Supplemental Material

Please note: The *Journal of Fish and Wildlife Management* is not responsible for the content or functionality of any supplemental material. Queries should be directed to the corresponding author for the article.

Table S1. Root mean-square error between each of the three images that we took with the Infrared Cameras, Inc. 9640 thermal camera at each elevation and vegetation combination after each image being clipped to just the area of the biobox. We took images of multiple bioboxes containing differing vegetative components and densities: (**C**) medium saltmeadow cordgrass *Spartina patens*; (**E**) dense sea rocket *Cakile edentula*; (**F**) medium mixed grasses and forbs, including saltmeadow cordgrass, smooth cordgrass *Spartina alterniflora*, sea rocket, and ragweed *Ambrosia* sp.; (**G**) sparse milkweed *Asclepsias* sp. Sparse = 30% cover, medium = 60% cover, and dense = 90% cover. Elevation is in meters. We collected all images in Millersville, Maryland on 9 June 2015.

Found at DOI: https://doi.org/10.3996/072019-JFWM-062.S1 (231 KB PDF).

Table S2. Comparison of beta regression models for explaining variation in the percentage of a domestic chicken chick *Gallus gallus* selected after digital processing of a thermal image. We took images with two cameras (FLIR Systems Tau-1 and Infrared Cameras, Inc. 9640) at each of five elevations (3, 6, 9, 10.5, and 12 m) and seven bioboxes containing differing vegetative components and densities: (**A**) no cover; (**B**) sparse saltmeadow cordgrass *Spartina patens*; (**C**) medium saltmeadow cordgrass; (**D**) dense saltmeadow cordgrass; (**E**) dense sea rocket *Cakile edentula*; (**F**) medium mixed grasses and forbs, including saltmeadow cordgrass and smooth cordgrass *Spartina alterniflora*, sea rocket, and ragweed *Ambrosia* sp.; (**G**) sparse milkweed *Asclepsias* sp. Sparse = 30% cover, medium = 60% cover, and dense = 90% cover. We collected all images in Millersville, Maryland on 9 June 2015 and processed them at thresholds of 115, 130, 145, 160, 175, 190, and 205.

Found at DOI: https://doi.org/10.3996/072019-JFWM-062.S2 (298 KB PDF).

Table S3. Full beta estimates describing the relationship among elevation, threshold, camera type, and biobox upon the percentage of a domestic chicken chick *Gallus gallus* selected by image processing. We took images with two cameras (FLIR Systems Tau-1 and Infrared Cameras, Inc. 9640) at each of five elevations (3, 6, 9, 10.5, and 12 m) and seven bioboxes containing differing vegetative components and densities: (**A**) no cover; (**B**) sparse saltmeadow cordgrass *Spartina patens*; (**C**) medium saltmeadow cordgrass; (**D**) dense saltmeadow cordgrass; (**E**) dense sea rocket *Cakile edentula*; (**F**) medium mixed grasses and forbs, including saltmeadow cordgrass and smooth cordgrass *Spartina alterniflora*, sea rocket, and ragweed *Ambrosia* sp.; (**G**) sparse milkweed *Asclepsias* sp. Sparse = 30% cover, medium = 60% cover, and dense = 90% cover. We collected all images in Millersville, Maryland on 9 June 2015 and processed them at thresholds of 115, 130, 145, 160, 175, 190, and 205.

Found at DOI: https://doi.org/10.3996/072019-JFWM-062.S3 (213 KB PDF).

Table S4. Comparison of binomial regression models for explaining variation in a human observer's ability to detect a domestic chicken chick *Gallus gallus* from a digitally processed thermal image. We took images with two cameras (FLIR Systems Tau-1 and Infrared Cameras, Inc. 9640) at each of five elevations (3, 6, 9, 10.5, and 12 m) and seven bioboxes containing differing vegetative components and densities: (**A**) no cover; (**B**) sparse saltmeadow cordgrass *Spartina patens*; (**C**) medium saltmeadow cordgrass; (**D**) dense saltmeadow cordgrass; (**E**) dense sea rocket *Cakile edentula*; (**F**) medium mixed grasses and forbs, including saltmeadow cordgrass and smooth cordgrass *Spartina alterniflora*, sea rocket, and ragweed *Ambrosia* sp.; (**G**) sparse milkweed *Asclepsias sp*. Sparse = 30% cover, medium = 60% cover, and dense = 90% cover. We collected all images in Millersville, Maryland on 9 June 2015 and processed them at thresholds of 115, 130, 145, 160, 175, 190, and 205.

Found at DOI: https://doi.org/10.3996/072019-JFWM-062.S4 (298 KB PDF).

Table S5. Full beta estimates describing the relationships among elevation, threshold, camera type, and biobox upon the ability of a human observer to detect a domestic chicken chick *Gallus gallus* in a digitally processed thermal image. We took images with two cameras: one forward-looking infrared (FLIR) camera, the FLIR Tau-1, from FLIR Systems, and one from the Infrared Cameras, Inc. 9640. We took images at each of five elevations (3, 6, 9, 10.5, and 12 m) and seven bioboxes containing differing vegetative components and densities: (**A**) no cover; (**B**) sparse saltmeadow cordgrass *Spartina patens*; (**C**) medium saltmeadow cordgrass; (**D**) dense saltmeadow cordgrass; (**E**) dense sea rocket *Cakile edentula*; (**F**) medium mixed grasses and forbs, including saltmeadow cordgrass and smooth cordgrass *Spartina alterniflora*, sea rocket, and ragweed *Ambrosia* sp.; (**G**) sparse milkweed *Asclepsias* sp. Sparse = 30% cover, medium = 60% cover, and dense = 90% cover. We collected all images in Millersville, Maryland on 9 June 2015 and processed them at thresholds of 115, 130, 145, 160, 175, 190, and 205.

Found at DOI: https://doi.org/10.3996/072019-JFWM-062.S5 (236 KB PDF).

Figure S1. Raw percentage of a domestic chicken chick *Gallus gallus* selected by FLIR Systems Tau-1 (FLIR) and Infrared Cameras, Inc. 9640 (ICI) cameras across elevation (in meters), threshold, and vegetation levels. The vegetation types are as follows: (**A**) no cover; (**B**) sparse saltmeadow cordgrass *Spartina patens*; (**C**) medium saltmeadow cordgrass; (**D**) dense saltmeadow cordgrass; (**E**) dense sea rocket *Cakile edentula*; (**F**) medium mixed grasses and forbs, including saltmeadow cordgrass and smooth cordgrass *Spartina alterniflora*, sea rocket, and ragweed *Ambrosia* sp.; (**G**) sparse milkweed *Asclepsias* sp. Sparse = 30% cover, medium = 60% cover, and dense = 90% cover. We collected all images in Millersville, Maryland on 9 June 2015.

Found at DOI: https://doi.org/10.3996/072019-JFWM-062.S6 (243 KB PDF).

Archived Material

Please note: The Journal of Fish and Wildlife Management *is not responsible for the content or functionality of any archived material. Queries should be directed to the corresponding author for the article.*

To cite this archived material, please cite both the journal article (formatting found in the Abstract section of this article) and the following recommended format for the archived material.

Data A1. All data for the analysis of percentage of chick selected and for chick detection at each threshold are contained in the Excel file (TIR_Data.csv).

Archived in the ScienceBase repository: https://doi.org/10.5066/P97UT9B7

Acknowledgments

Funding for this project was provided by the U.S. Geological Survey (Ecosystems Mission Area) and UAS-Bio, llc. The authors thank B. Ho-Sung Lee for field assistance and J. Tassone for comments on earlier versions of this manuscript, as well as the Associate Editor and anonymous journal reviewers for their constructive feedback throughout the review process. Protocols for handling live birds were approved by the U.S. Geological Survey Patuxent Wildlife Research Center Animal Care and Use Committee (No. 2015-04).

Any use of trade, product, website, or firm names in this publication is for descriptive purposes only and does not imply endorsement by the U.S. Government.

References

Abd-Elrahman A, Pearlstine L, Percival F. 2005. Development of pattern recognition algorithm for automatic bird detection from unmanned aerial vehicle imagery. Surveying and Land Information Science 65:37–45.

Andes AK, Buckley BR, Warren TL, Woods PC, Yancey SR, Dabbert CB. 2012. Use of a thermal camera to aid in capturing northern bobwhite quail chicks. Wildlife Society Bulletin 36:371–375.

Benshemesh JS, Emison WB. 1996. Surveying malleefowl breeding densities using an airborne thermal scanner. Wildlife Research 23:121–142.

Betke M, Hirsh DE, Bagchi A, Hristov NI, Makris NC, Kunz TH. 2007. Tracking large variable numbers of objects in clutter. IEEE Conference on Computer Vision and Pattern Recognition 1–8.

Betke M, Hirsh DE, Makris NC, McCracken GF, Procopio M, Hristov NI, Tang S, Bagchi A, Reichard JD, Horn JW, Crampton S, Cleveland CJ, Kunz TH. 2008. Thermal imaging reveals significantly smaller Brazilian free-tailed bat colonies than previously estimated. Journal of Mammalogy 89:18–24.

Bibby CJ, Buckland ST. 1987. Bias of bird census results due to detectability varying with habitat. Acta Oecologica 8:103–112.

Boonstra RJ, Eadie M, Krebs CJ, Boutin S. 1995. Limitations of far infrared thermal imaging in locating birds. Journal of Field Ornithology 66:192–198.

Butler DA, Ballard WB, Haskell SP, Wallace MC. 2006. Limitations of thermal infrared imaging for locating neonatal deer in semiarid shrub communities. Wildlife Society Bulletin 34:1458–1462.

Carney KM, Sydeman WJ. 1999. A review of human disturbance effects on nesting colonial waterbirds. Waterbirds 22:68–79.

Chabot D, Bird DM. 2012. Evaluation of an off-the-shelf unmanned aircraft system for surveying flocks of geese. Waterbirds 35:170–174.

Chabot D, Craik SR, Bird DM. 2015. Population census of a large common tern colony with a small unmanned aircraft. PLoS ONE 10:1–14.

Chen CK, Chuang HF, Wu SM, Li WH. 2019. Feather evolution from precocial to altricial birds. Zoological Studies 58. https://doi.org/10.6620/ZS.2019.58-24

Cribari-Neto F, Zeileis A. 2010. Beta regression in R. Journal of Statistical Software 34:1–24.

Erwin RM. 1989. Responses to human intruders by birds nesting in colonies: experimental results and management guidelines. Colonial Waterbirds 12:104–108.

Galligan EW, Bakken GS, Lima SL. 2003. Using a thermographic imager to find nests of grassland birds. Wildlife Society Bulletin 31:865–869.

Gates DM, Keegan HJ, Schleter JC, Weidner VR. 1965. Spectral properties of plants. Applied Optics 4:11–20.

Hanson L, Holmquist-Johnson CL, Cowardin ML. 2014. Evaluation of the Raven sUAS to detect and monitor greater sage-grouse leks within the Middle Park population (No. 2014–1205). Washington, D.C.: U.S. Geological Survey.

Hodgson JC, Baylis SM, Mott R, Herrod A, Clarke RH. 2016. Precision wildlife monitoring using unmanned aerial vehicles. Scientific Reports 6:22574.

Hristov NI, Betke M, Kunz TH. 2008. Applications of thermal infrared imaging for research in aeroecology. Integrative and Comparative Biology 48:50–59.

Hutt M. 2011. Utilizing UAS Raven to estimate sandhill crane abundance. USGS—science for a changing world 11.

Jenks-Jay N. 1982. Chick shelters decrease avian predation in least tern colonies on Nantucket Island, Massachusetts. Journal of Field Ornithology 53:58–60.

Kinzel PJ, Nelson JM, Parker RS, Davis LR. 2006. Spring census of mid-continent Sandhill Cranes using aerial infared videography. Journal of Wildlife Management 70:70–77.

Linchant J, Lisein J, Semeki J, Lejeune P, Vermeulen C. 2015. Are unmanned aircraft systems (UASs) the future of wildlife monitoring? A review of accomplishments and challenges. Mammal Review 45:239–252.

Locke SL, Lopez RR, Peterson MJ, Silvy NJ, Schwertner TW. 2006. Evaluation of portable infrared cameras for detecting Rio Grande Wild Turkeys. Wildlife Society Bulletin 34:839–844.

Maryland Natural Heritage Program. 2016. List of rare, threatened, and endangered animals of Maryland. Annapolis: Maryland Department of Natural Resources,.

McCafferty DJ. 2013. Applications of thermal imaging in avian science. Ibis 155:4–15.

McCafferty DJ, Moncrieff JB, Taylor IR, Boddie GF. 1998. The use of IR thermography to measure the radiative temperature and heat loss of a barn owl (*Tyto alba*). Journal of Thermal Biology 23:311–318.

Mills WE, Harrigal DE, Owen SF, Dukes WF, Barrineau DA, Wiggers EP. 2011. Capturing clapper rails using thermal imaging technology. Journal of Wildlife Management 75:1218–1221.

Mirzaei G, Jamali MM, Ross JD, Gorsevski PV, Bingman VP. 2014. Fuzzy clustering in avian infrared imagery application. IEEE International Conference on Electro Information Technology 236–239.

Mirzaei G, Majid MW, Ross J, Jamali MM, Gorsevski PV, Frizado JP, Bingman VP. 2012. Avian detection & tracking algorithm using infrared imaging. 2012 IEEE International Conference on Electro/Information Technology 1–4.

Mulroy TW. 1979. Spectral properties of heavily glaucous and non-glaucous leaves of a succulent rosette-plant. Oecologia 38:349–357.

Nisbet ICT, Arnold JM, Oswald SA, Pyle P, Patten MA. 2017. Common tern (*Sterna hirundo*), version 3.0. In Rodewald PG, editor. The birds of North America. Ithaca, New York: Cornell Lab of Ornithology.

Owen PA. 2011. When the ravens met the sandhill cranes: USGS and USFWS team turns to unmanned aircraft to count wildlife. Unmanned Systems 29:20–33.

Palmer RS. 1941. A behavior study of the Common Tern (*Sterna hirundo*). Boston: Boston Society of Natural History.

Reintsma KM, McGowan PC, Callahan C, Collier T, Gray D, Sullivan JD, Prosser DJ. 2018. Preliminary evaluation of behavioral response of nesting waterbirds to small unammed aircraft flight. Waterbirds 41:326–331.

Ricklefs RE. 1979. Patterns of growth in birds V. A comparitive study of development in the starling, common tern, and Japanese quail. Auk 96:10–30.

Rodgers JA, Smith HT. 1995. Set-back distances to protect nesting bird colonies from human disturbance in Florida. Conservation Biology 9:89–99.

Smithson M, Verkuilen J. 2006. A better lemon squeezer? Maximum-likelihood regression with beta-dsitributed dependent variables. Psychological Methods 11:54–71.

Steen KA, Villa-Henriksen A, Therkildsen OR, Green O. 2012. Automatic detection of animals in mowing operations using thermal cameras. Sensors 12:7587–7597.

Steinkamp M, Peterjohn B, Byrd V, Carter H, Lowe, R. 2003. Breeding season survey techniques for seabirds and colonial waterbirds throughout North America. Laurel, Maryland: U.S. Geological Survey Patuxent Wildlife Research Center.